Analytical characterization of the dynamic response of viscoelastic metamaterials

Valappil, Sabiju Valiya; Krushynska, Anastasiia; Aragón, Alejandro M.

Published in:
Computational Materials Science

DOI:
10.1016/j.commatsci.2023.112385

Publication date:
2023

Computational Materials Science 229 (2023) 112385

Contents lists available at ScienceDirect

Computational Materials Science

journal homepage: www.elsevier.com/locate/commatsci

Full length article

Analytical characterization of the dynamic response of viscoelastic metamaterials

Sabiju Valiya Valappil [a,1], Anastasiia O. Krushynska [b], Alejandro M. Aragón [a,*,2]

[a] Faculty of Mechanical, Maritime and Materials Engineering, Delft University of Technology, Mekelweg 2, 2628 CD Delft, The Netherlands
[b] Engineering and Technology Institute Groningen, Faculty of Science and Engineering, University of Groningen, Nijenborgh 4, Groningen 9747AG, The Netherlands

ARTICLE INFO

Keywords:
Elastic metamaterials
Spectral element method
Viscoelastic damping
Analytical modeling
Band structure
Transmissibility
Dynamic experiments
Generalized Maxwell model

ABSTRACT

The band-gap frequencies of elastic metamaterials are ideally determined by a metamaterial architecture; yet, in practical situations, are often dependent on the material damping in their constituent(s). The analysis of viscoelastic metamaterials requires however substantial computational resources and, except for oversimplified cases, is solely done numerically. Here, we propose an analytical procedure based on the spectral element method (SEM) to analyze bulk metamaterials with viscoelastic damping as continuous systems. Due to intrinsic limitations of the SEM to deal with complex geometries, we develop a procedure to build an approximate model based on SEM frame elements. The viscoelastic behavior is included by means of complex viscoelasticity moduli expressed by the generalized Maxwell mechanical model. We validate this approach by analyzing metamaterial plates and verify the findings experimentally. We demonstrate that our SEM-based analytical model can accurately capture wave transmission around the first band-gap frequencies. Therefore, our extension of the SEM approach to analyze three-dimensional meta-structures is promising to characterize wave propagation in realistic viscoelastic structures (with any type of linear viscoelastic behavior) in an accurate and computationally efficient way.

1. Introduction

Damping is an intrinsic property of real-world dynamic systems that reduces, restricts, and even prevents oscillations [1]. Although damping is beneficial in vehicle suspension systems [2], seismic isolation [3], and sound or vibration mitigation [4], among others, high damping values can detrimentally amplify higher-frequency resonance modes [5], decrease the quality factor of resonators [6], and generate heat in high-speed systems [7,8]. Damping has a complex nature and different origins. Material damping is caused, for example, by internal losses due to defects and impurities at the microstructural level. Structural damping is due to friction in joints and semi-rigid connections. Other forms of damping are thermoelastic damping, where a gradient in local temperature leads to energy dissipation, and fluid damping, where energy loss is due to drag resistance in a fluid. In this study, we consider damping due to viscoelastic material behavior, which can be represented by the imaginary components of complex-values elasticity moduli [9]. Viscoelastic damping, being an intricate subject in material science and rheology by itself [10], becomes even more challenging to analyze when superimposed on the dynamic effects governed by the material architecture. This occurs in elastic metamaterials.

Elastic metamaterials are architected materials with frequency band gaps where the propagation of mechanical waves is forbidden. This peculiar functionality, not typical for most conventional engineering materials, is achieved due to destructive interference of waves at material interfaces or boundaries [11]. In periodic structures, this process is similar to the Bragg scattering of electromagnetic waves [12] and occurs at frequencies when the corresponding wavelength is comparable with a characteristic dimension of a lattice. Alternatively, destructive interference can be induced by Mie (resonance-type) scattering near a resonance frequency of embedded resonators enabling the break of the periodicity restriction [13].

Large application potential of elastic metamaterials, including vibration isolation [14], acoustic diodes and transistors [15,16], energy harvesting [17], acoustic lenses [18,19], acoustic antennas [20], frequency steering [21,22], acoustic cloaking [23–26], and other acoustic devices [27], requires accurate prediction of their wave propagation characteristics. This implies considering realistic material behavior while analyzing the dynamics of elastic metamaterials. For intrinsically viscoelastic polymer meta-structures, the dynamic analysis is

* Corresponding author.
E-mail addresses: S.ValiyaValappil@tudelft.nl (S. Valiya Valappil), a.o.krushynska@rug.nl (A.O. Krushynska), a.m.aragon@tudelft.nl (A.M. Aragón).
[1] www.tudelft.nl/en/3me/about/departments/precision-and-microsystems-engineering-pme/people/junior-research-staff/valiya-valappil-sabiju/
[2] 3me.tudelft.nl/aaragon

https://doi.org/10.1016/j.commatsci.2023.112385
Received 9 February 2023; Received in revised form 11 July 2023; Accepted 12 July 2023
Available online 25 July 2023

not straightforward due to the complexity of lossy material behavior and the abundance of viscoelastic models with not readily available parameters. These complications are further aggravated by high computational costs due to doubled size of the stiffness and mass matrices in finite-element simulations. Additionally, the frequency-dependent viscoelasticity can drastically alter the dynamic response of viscoelastic metamaterials by changing the positions of pass and stop bands thus modifying the width and frequencies of band gaps [28,29]. Therefore, proper analysis of viscoelastic metamaterials requires the knowledge of viscoelastic models, time- and resource-efficient approaches, and, simultaneously, should be accurate enough to reliably predict experimentally observed dynamics.

Currently available models to study the wave dynamics in viscoelastic metamaterials can be loosely classified into discrete lumped-mass [30], discretized distributed-mass [31], and continuous distributed-mass models [32]. The discrete lumped-mass models, in which a host medium and scatterers/resonators are represented as interconnected springs, dashpots, and point masses, can capture the viscoelastic damping. They are straightforward to implement and computationally inexpensive [33–36], can be extended to include nonlinear behavior [37] or multiple resonators/scatterers [38], and have been used to model damped metamaterials in various applications [39–41]. However, the accuracy of these models is inherently limited to a low-frequency range, *i.e.,* to frequencies below the first band gap. Distributed-mass models (discretized and continuous) consider the geometry of viscoelastic metamaterials as is that allows adequate capturing of the wave dynamics at various frequency ranges. A representative example is the finite element method (FEM) [42] that has been extensively used to analyze damped metamaterials of complex geometries [43–49]. The finite element models are though computationally expensive as they require–as a rule of thumb–more than six linear elements to represent the wavelength accurately [50], and thus the degrees of freedom (DOFs) drastically increase with frequency and because of the complex-valued problem formulation. As a result, finite-element simulations are incredibly costly in terms of memory and computational time. To overcome this, Shi et al. [51,52] proposed the time-dependent spectral element method (*t*-SEM), whereby using high-order polynomials (Gauss–Lobatto–Legendre basis functions) to define the approximation that greatly improved computational efficiency [53,54]. For the same target frequency, *t*-SEM shows a significant reduction in the number of finite elements when compared to standard finite element formulation based on linear shape functions.

The two discussed classes of analysis approaches imply the discretization of the equations of motion. This step is however not needed (or at least not entirely) in continuous distributed-mass methods, including the spectral element method (SEM) [55]. The SEM, which is completely unrelated to *t*-SEM, is an analytical method based on fast or discrete Fourier transform techniques (FFT/DFT) [56] that has mainly been used to solve wave propagation problems. It does not have a limitation with respect to frequency because the employed shape functions are solutions to the wave equations. Because of this, SEM has been applied in analyses of flow-induced vibrations in pipes [57], axially moving structures [58], dynamics of multi-layer and smart structures [59], and the identification of cracks and joints [59], among others. The viscoelasticity can easily be incorporated into an SEM model by means of complex-valued elasticity moduli. SEM has the potential to predict the dynamics of viscoelastic metamaterials accurately with low computational cost, as has been successfully shown for 1D meta-structures [60–65]. However, the extension to two- or three-dimensional structures is not straightforward as the SEM cannot directly solve nonlinear problems [59] and deal with complex geometries due to the unavailability of corresponding solutions to the wave equations. To the best of our knowledge, nowadays there are no studies on the dynamics of viscoelastic metamaterials of complex geometries by means of SEM or any other similar techniques that can provide reliable predictions.

In this work, we extend SEM to study the dynamics of bulk and plate-like viscoelastic meta-structures and prove that it accurately predicts the wave dynamics below and above the first band gap with little to no computational costs. Our approach relies on approximating the geometry of a representative unit cell of a viscoelastic metamaterial by a combination of the SEM frame elements and incorporating the viscoelastic behavior by a generalized Maxwell model, which fits experimentally measured master curves of a viscoelastic polymer. The predicted results are validated in transmission experiments performed on polycarbonate metamaterial plates.

2. Spectral element method for wave propagation analysis of viscoelastic systems

We begin by describing the steps of the general procedure to study the wave propagation by means of the SEM as also outlined in the flowchart in Fig. 1. First, one needs to represent (approximate) the geometry of an analyzed structure by means of *spectral elements* such as bars, beams, plates, or other elements, for which solutions to the wave equations are available (or can be derived). Next, the equations of motion are transformed from the time domain to the frequency domain using FFT/DFT. These equations are formulated in terms of complex-valued elastic moduli in order to describe the viscoelastic material behavior and then solved to obtain the shape functions. Using these functions, one can derive the dynamic stiffness matrix (DSM) for each spectral element, which enters a global DSM. The assembly process of the global DSM is similar to that in the standard FEM. Further, one can solve the system equations under appropriate boundary conditions to obtain the required response. In the case of a linear viscoelastic behavior, such as the one described in the present study, the viscoelastic model can be introduced after deriving the shape functions and only then incorporated into the DSM.

2.1. SEM model for 3D viscoelastic metamaterials

In this section, we apply the described procedure to study the dynamics of bulk elastic metamaterials. For this, we consider a general elastic metamaterial configuration shown in Fig. 2. The constituent cylinders can be considered as frame elements with 12 DOFs responsible for axial, bending, and torsional deformations as indicated in the inset of Fig. 2. The dynamics of these elements can be approximated by that of the Euler–Bernoulli beam, with the viscoelastic behavior incorporated in the complex-valued elasticity moduli [66].

The equations of motion that govern the wave propagation in a corresponding 1D viscoelastic frame element in the absence of a source term are those that represent the propagation of longitudinal (axial component), flexural (bending component), and twisting (torsional component) waves, respectively:

$$\hat{E}(\imath\omega)\,A\frac{\partial^2 u}{\partial x^2}-\rho A\frac{\partial^2 u}{\partial t^2}=0,\qquad \hat{E}(\imath\omega)\,I_{xx}\frac{\partial^4 w}{\partial x^4}-\rho A\frac{\partial^2 w}{\partial t^2}=0,$$
$$\hat{G}(\imath\omega)\,J\frac{\partial^2 \theta}{\partial x^2}-\rho J\frac{\partial^2 \theta}{\partial t^2}=0. \tag{1}$$

Here u, w, and θ are the axial, flexural, and torsional DOFs of the frame element; x and t are the spatial coordinate and time; ρ is the density, $\hat{E}(\imath\omega)$ and $\hat{G}(\imath\omega)$ are the complex-valued Young's and shear moduli with $\imath$ denoting the imaginary number; ω is frequency; A is the cross-sectional area; I_{xx} is the second moment of area w.r.t. x axis, and J is the second polar moment of area of the frame element. Note that w represents the flexural displacement that can capture only bending with respect to the x axis. Similar equation to capture the bending with respect to the y axis can be obtained by replacing w, x, and I_{xx} in the second equation of Eq. (1) with v, y, and I_{yy}, respectively. The complex Young's modulus and shear modulus are represented as [47]:

$$\hat{E}(\imath\omega)=E_\infty+\sum_{i=1}^{n}\frac{\imath\omega E_i}{\imath\omega\tau_i+1},\qquad \hat{G}(\imath\omega)=\frac{\hat{E}(\imath\omega)}{2(1+\nu)} \tag{2}$$

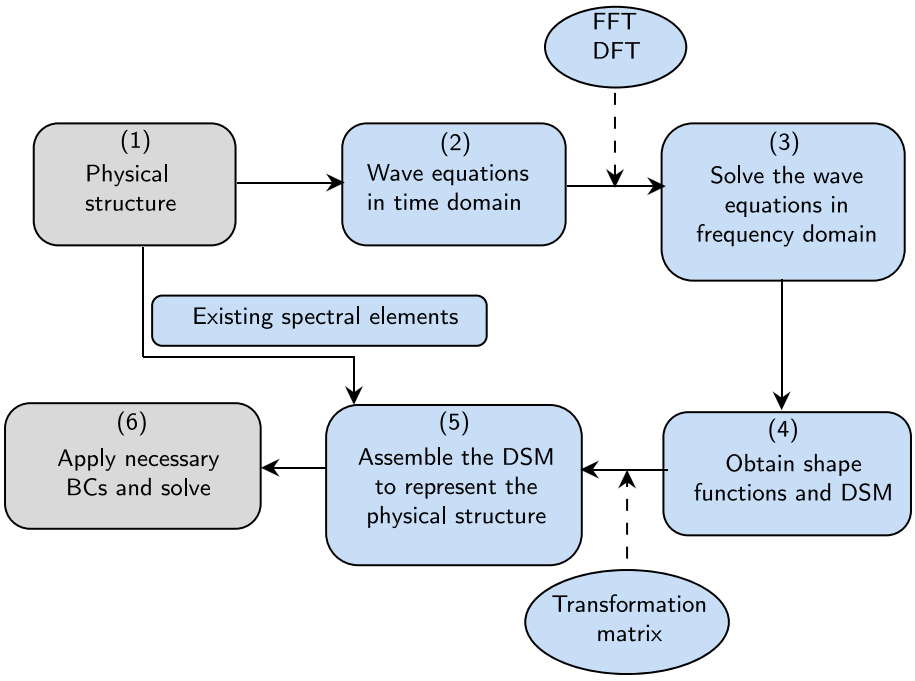

Fig. 1. Flowchart representing the general SEM process for analyzing wave propagation through a structure starting from the physical structure till solving the DSM after applying BCs. The viscoelastic model can either be introduced in step 3 before solving the EOM or, in the case of a linear viscoelastic system, during step 4 after obtaining the shape functions.

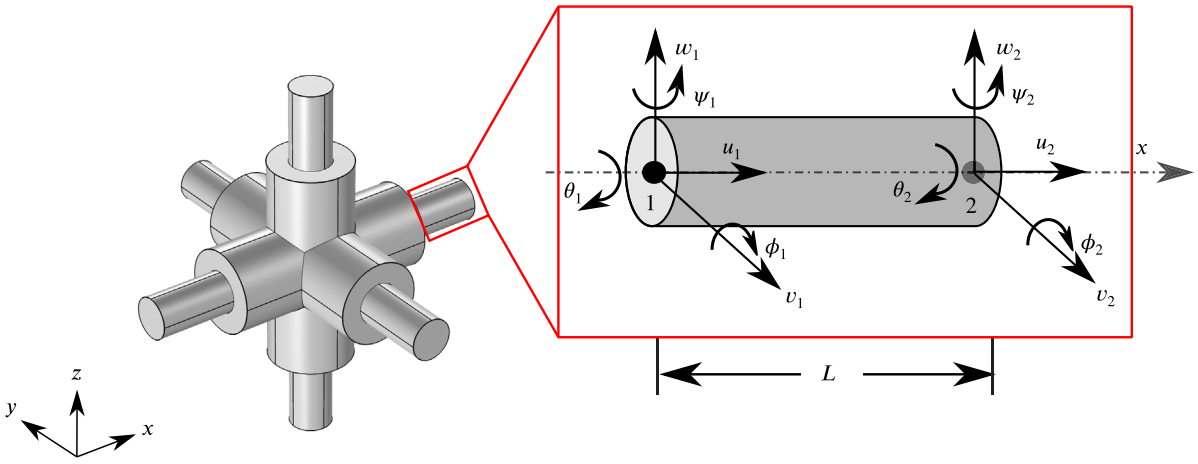

Fig. 2. A three-dimensional metamaterial unit cell that can be represented by a collection of a two-node frame element shown in the inset. The frame element of length L has 6 DOFs per node corresponding to axial, bending, and torsional deformations.

where $\tau_i = \eta_i / E_i$ and E_i denote, respectively, the ith Maxwell element's relaxation time and relaxation modulus, η_i is the dynamic viscosity, E_∞ is Young's modulus at equilibrium, and ν is the Poisson's ratio, which is assumed to be constant. The number n is usually chosen to ensure adequate fit with experimental data.

We consider two boundary-value problems (BVPs) corresponding to the following analysis cases:

1. **BVP 1: Band structure analysis** implies the study of the dispersion relation. This relation is obtained by solving an eigenvalue problem for a metamaterial unit cell subject to Bloch–Floquet boundary conditions with the wave vector values restricted to the irreducible Brillouin zone [67]. These boundary conditions in our case take the following form:

$$\boldsymbol{u}(\underline{x} + \boldsymbol{a}_i, t) = e^{i(\boldsymbol{k}.\boldsymbol{a}_i)}\boldsymbol{u}(\underline{x}, t), \tag{3}$$

where $\boldsymbol{u}$ is the DOF vector that includes all displacements and rotations, $\underline{x}$ is the position vector, and $\boldsymbol{a}_i$ is the lattice vector along the ith coordinate. For the band structure analysis, we use the $\omega(\boldsymbol{k})$ approach that implies calculating frequencies for a fixed $\boldsymbol{k}$.

2. **BVP 2: Transmission analysis** allows studying wave characteristics in finite-size structures by performing the steady-state dynamic analysis of a metamaterial waveguide under the Dirichlet boundary conditions [68]:

$$\boldsymbol{u}(\underline{l}, t) = \tilde{\boldsymbol{u}} e^{i\omega t}, \tag{4}$$

where $\tilde{\boldsymbol{u}}$ is the prescribed displacement amplitude at location $\underline{x} = \underline{l}$. The wave transmission can be estimated as a ratio of the output displacement to the input displacement for the frequency range of interest.

$$\boldsymbol{s}(\omega)=\begin{bmatrix}
s_{A11} & 0 & 0 & 0 & 0 & 0 & s_{A12} & 0 & 0 & 0 & 0 & 0\\
0 & s_{Bx11} & 0 & 0 & s_{Bx12} & 0 & 0 & s_{Bx13} & 0 & 0 & s_{Bx14} & 0\\
0 & 0 & s_{By11} & 0 & 0 & s_{By12} & 0 & 0 & s_{By13} & 0 & 0 & s_{By14}\\
0 & 0 & 0 & s_{T11} & 0 & 0 & 0 & 0 & 0 & s_{T12} & 0 & 0\\
0 & s_{Bx12} & 0 & 0 & s_{Bx22} & 0 & 0 & s_{Bx23} & 0 & 0 & s_{Bx24} & 0\\
0 & 0 & s_{By12} & 0 & 0 & s_{By22} & 0 & 0 & s_{By23} & 0 & 0 & s_{By24}\\
s_{A12} & 0 & 0 & 0 & 0 & 0 & s_{A22} & 0 & 0 & 0 & 0 & 0\\
0 & s_{Bx13} & 0 & 0 & s_{Bx23} & 0 & 0 & s_{Bx33} & 0 & 0 & s_{Bx34} & 0\\
0 & 0 & s_{By13} & 0 & 0 & s_{By23} & 0 & 0 & s_{By33} & 0 & 0 & s_{By34}\\
0 & 0 & 0 & s_{T12} & 0 & 0 & 0 & 0 & 0 & s_{T22} & 0 & 0\\
0 & s_{Bx14} & 0 & 0 & s_{Bx24} & 0 & 0 & s_{Bx34} & 0 & 0 & s_{Bx44} & 0\\
0 & 0 & s_{By14} & 0 & 0 & s_{By24} & 0 & 0 & s_{By34} & 0 & 0 & s_{By44}
\end{bmatrix}, \tag{8}$$

Box I. DSM for a single frame element in space.

The shape functions satisfying Eq. (1) for longitudinal waves can be represented as follows [59]:

$$\boldsymbol{N}_L(x,\omega)=\begin{bmatrix}\csc\left(k_L L\right)\sin\left[k_L(L-x)\right] & \csc\left(k_L L\right)\sin\left(k_L x\right)\end{bmatrix}, \tag{5}$$

where $k_L = \|\boldsymbol{k}_L\| = \omega/C_L$ is the magnitude of the longitudinal wave vector along the wave propagation direction and $C_L = \sqrt{\hat{E}(\imath\omega)/\rho}$ is the longitudinal wave velocity. For flexural waves, the shape functions can be represented as follows:

$$\begin{aligned}
&\boldsymbol{N}_B(x,\omega) = [N_{B1} \quad N_{B2} \quad N_{B3} \quad N_{B4}],\\
&N_{B1}(x,\omega) = \eta^{-1}k_{Fx}[\cos\bar{x} - \cos(\bar{L}_x-\bar{x})\cosh\bar{L}_x - \cos\bar{L}_x\cosh(\bar{L}_x-\bar{x})\\
&\qquad + \cosh\bar{x} + \sin(\bar{L}_x-\bar{x})\sinh\bar{L}_x - \sin\bar{L}_x\sinh(\bar{L}_x-\bar{x})],\\
&N_{B2}(x,\omega) = \eta^{-1}[-\cosh(\bar{L}_x-\bar{x})\sin\bar{L}_x + \cosh\bar{L}_x\sin(\bar{L}_x-\bar{x}) + \sin\bar{x}\\
&\qquad - \cos(\bar{L}_x-\bar{x})\sinh\bar{L}_x + \cos\bar{L}_x\sinh(\bar{L}_x-\bar{x}) + \sinh\bar{x}],\\
&N_{B3}(x,\omega) = \eta^{-1}k_{Fx}[\cos(\bar{L}_x-\bar{x}) - \cos\bar{x}\cosh\bar{L}_x - \cos\bar{L}_x\cosh\bar{x}\\
&\qquad + \cosh(\bar{L}_x-\bar{x}) + \sin\bar{x}\sinh\bar{L}_x - \sin\bar{L}_x\sinh\bar{x}],\\
&N_{B4}(x,\omega) = -\eta^{-1}[-\cosh\bar{x}\sin\bar{L}_x + \cosh\bar{L}_x\sin\bar{x} + \sin(\bar{L}_x-\bar{x})\\
&\qquad - \cos\bar{x}\sinh\bar{L}_x + \cos\bar{L}_x\sinh\bar{x} + \sinh(\bar{L}_x-\bar{x})].
\end{aligned} \tag{6}$$

where $\eta = 2k_{Fx}(1-\cos\bar{L}_x\cosh\bar{L}_x)$, $\bar{x} = k_{Fx}x$, and $\bar{L}_x = k_{Fx}L$ are introduced for brevity, $k_{Fx} = \|\boldsymbol{k}_{Fx}\| = \sqrt{\omega}\left(\frac{\rho A}{\hat{E}(\imath\omega)I_{xx}}\right)^{1/4}$ is the magnitude of the flexural wave vector along the x axis, $C_{Fx} = \left(\frac{\hat{E}(\imath\omega)I_{xx}}{\rho A}\right)^{1/4}$ is the velocity of flexural waves. The shape functions for bending waves along the y axis can be obtained from Eq. (6) by replacing x with y, I_{xx} with I_{yy}, and $\boldsymbol{k}_{Fx}$ with $\boldsymbol{k}_{Fy}$. For torsional waves, the shape functions take the form:

$$\boldsymbol{N}_T(x,\omega)=\begin{bmatrix}\csc\left(k_T L\right)\sin\left[k_T(L-x)\right] & \csc\left(k_T L\right)\sin\left(k_T x\right)\end{bmatrix}, \tag{7}$$

where $k_T = \|\boldsymbol{k}_T\| = \omega/C_T$ is the magnitude of the torsional wave vector and $C_T = \sqrt{\hat{G}(\imath\omega)/\rho}$ is the torsional wave velocity. Note that wave velocities C_L, C_F, and C_T are functions of frequency and thus correspond to dispersive waves, in contrast to the undamped situation when C_L and C_T are constants. Since the shape functions implicitly contain these wave velocities, the dispersive behavior is accurately captured by SEM.

The DSM for a single frame element can then be obtained by using the derived shape functions as given in (see [59] for more details) Box I, where the longitudinal waves are described by the following stiffness components:

$$\begin{aligned}
s_{A11} &= s_{A22} = \hat{E}(\imath\omega)\,Ak_A\cot\left(k_A L\right),\\
s_{A12} &= -\hat{E}(\imath\omega)\,Ak_A\csc\left(k_A L\right).
\end{aligned} \tag{9}$$

The flexural x-polarized waves are described by the other set of stiffness components:

$$\begin{aligned}
s_{Bx11} &= s_{Bx33} = \Delta_{Bx}\bar{L}_x^3(\cos\bar{L}_x\sinh\bar{L}_x + \sin\bar{L}_x\cosh\bar{L}_x),\\
s_{Bx22} &= s_{Bx44} = \Delta_{Bx}\bar{L}_x^3k_{Fx}^{-2}(-\cos\bar{L}_x\sinh\bar{L}_x + \sin\bar{L}_x\cosh\bar{L}_x),\\
s_{Bx12} &= -s_{Bx34} = \Delta_{Bx}\bar{L}_x^3k_{Fx}^{-1}\sin\bar{L}_x\sinh\bar{L}_x,\\
s_{Bx13} &= -\Delta_{Bx}\bar{L}_x^3(\sin\bar{L}_x + \sinh\bar{L}_x),\\
s_{Bx14} &= -s_{B23} = \Delta_B\bar{L}_x^3k_F^{-1}(-\cos\bar{L}_x + \cosh\bar{L}_x),\\
s_{Bx24} &= \Delta_B\bar{L}_x^3k_F^{-2}(-\sin\bar{L}_x + \sinh\bar{L}_x),
\end{aligned} \tag{10}$$

with $\Delta_{Bx} = \frac{1}{1-\cos\bar{L}_x\cosh\bar{L}_x}$. The corresponding stiffness components for flexural y-polarized waves are obtained from Eq. (10) by replacing $\bar{L}_x$ with $\bar{L}_y$, $\boldsymbol{k}_{Fx}$ with $\boldsymbol{k}_{Fy}$, and Δ_{Bx} with Δ_{By}. Finally, the torsional stiffness components are:

$$\begin{aligned}
s_{T11} &= s_{T22} = \hat{G}(\imath\omega)\,Jk_T\cot\left(k_T L\right),\\
s_{T12} &= -\hat{G}(\imath\omega)\,Jk_T\csc\left(k_T L\right).
\end{aligned} \tag{11}$$

2.1.1. Dynamic stiffness matrix of the 3D viscoelastic metamaterial

The global DSM is obtained by assembling individual DSMs of each frame element considering its orientation. To that end, we use the following rotation matrices [69]:

$$\boldsymbol{T}=\begin{bmatrix}\boldsymbol{Q} & \boldsymbol{0} & \boldsymbol{0} & \boldsymbol{0}\\ \boldsymbol{0} & \boldsymbol{Q} & \boldsymbol{0} & \boldsymbol{0}\\ \boldsymbol{0} & \boldsymbol{0} & \boldsymbol{Q} & \boldsymbol{0}\\ \boldsymbol{0} & \boldsymbol{0} & \boldsymbol{0} & \boldsymbol{Q}\end{bmatrix},\quad \boldsymbol{Q}=\begin{bmatrix}\boldsymbol{n}_{x1} & \boldsymbol{n}_{x2} & \boldsymbol{n}_{x3}\\ \boldsymbol{n}_{y1} & \boldsymbol{n}_{y2} & \boldsymbol{n}_{y3}\\ \boldsymbol{n}_{z1} & \boldsymbol{n}_{z2} & \boldsymbol{n}_{z3}\end{bmatrix},\quad \bar{\boldsymbol{s}}_1 = \boldsymbol{T}^{\intercal}\times\boldsymbol{s}_1\times\boldsymbol{T}, \tag{12}$$

where $\boldsymbol{n}_x = \frac{1}{L}\{x_2-x_1 \quad y_2-y_1 \quad z_2-z_1\}$, $\boldsymbol{n}_y = \frac{1}{\sqrt{n_{x1}^2+n_{x2}^2}}\{-n_{x2} \quad n_{x1} \quad 0\}$, and $\boldsymbol{n}_z = \boldsymbol{n}_x\times\boldsymbol{n}_y$ are directional cosines and $\{x,y,z\}$ is the coordinate system of the frame element's node (see Fig. 2). The global DSM for the unit cell shown in Fig. 2 has thus 78 DOFs (12 frame elements) and can be used to estimate the band structure when combined with Eq. (3) or to estimate wave transmission using Eq. (4).

To analyze the dynamics of a viscoelastic metamaterial, one needs to introduce an appropriate damping model into the DSM. In the next section, we discuss how it can be done.

2.1.2. Viscoelastic mechanical models

Complex elastic moduli describing viscoelastic behavior have the real part – storage modulus – representing elastic behavior and the imaginary part – loss modulus – describing viscous losses. The ratio of the loss modulus to the storage modulus is known as the loss factor (or loss tangent) and provides a measure of energy dissipation in a material. The dependence of the viscoelastic properties (storage modulus, loss modulus, and loss factor) on frequency, temperature, strain-rate,

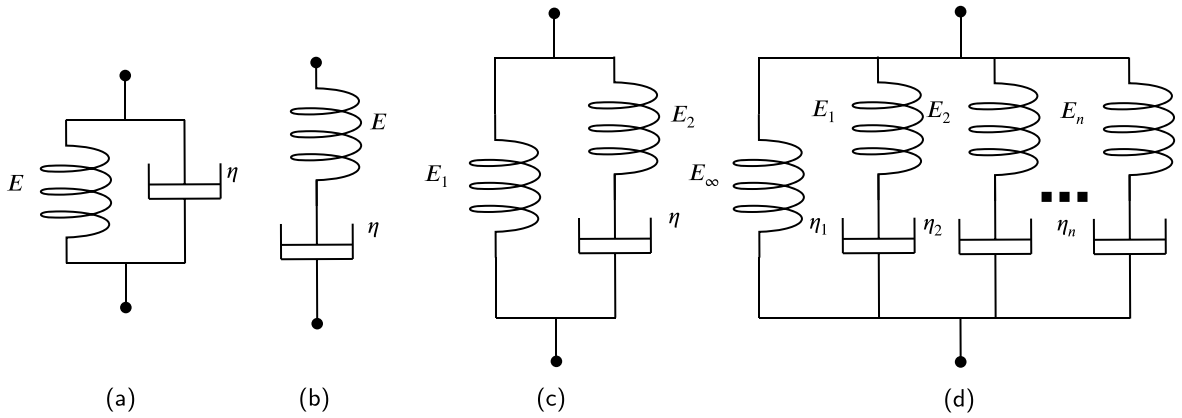

Fig. 3. Linear viscoelastic models with their parameters. (a) Kelvin–Voigt, (b) Maxwell, (c) Zener, and (d) generalized Maxwell models. E_i and η_i, respectively, represent the relaxation modulus and damping factor of the i^{th} Maxwell element, while E_∞ is the elastic modulus at equilibrium.

creep, pre-load [70], and aging [71] complicates the material characterization and quantification of the moduli. To address this challenge, it was proposed to use several simplified models, *e.g.*, Kelvin–Voigt [72], Zener [73], and Maxwell [74] models as shown in Fig. 3. The Kelvin–Voigt and Maxwell models represented by a spring and a dashpot connected in parallel and in series, respectively, are widely used [75], but cannot capture the viscoelastic behavior of any real material. The Zener model is an extension of the Kelvin–Voigt model with an added spring to represent the elastic behavior at equilibrium. Despite being more accurate, this model is still oversimplified for practical situations. More accurate approximations of viscoelastic material response can be obtained by combining several Maxwell or Kelvin–Voigt elements together that result in generalized models, for instance, the generalized Maxwell model shown in Fig. 3(d), which are typically used to fit experimentally measured values of the storage and loss moduli [76].

2.2. SEM vs FEM for viscoelastic problems

Here, we incorporate the generalized Maxwell viscoelastic model into the DSM by replacing elastic moduli in Eqs. (8)–(11) with Eq. (2). As explained, the values of the relaxation moduli and relaxation times for the Maxwell elements in Eq. (2) can be obtained by fitting them into experimentally measured master curves [76]. Since in SEM, the wave vector is a function of the material moduli, variations in the moduli values are immediately reflected in the wave vector and, thus, in the elements of the DSM. Therefore, at every analyzed frequency, the constituents of the DSM change according to the viscoelastic behavior reflected by the viscoelastic moduli values, ensuring accurate predictions. This is in contrast to the FEM analysis, where the viscoelastic moduli do not enter the interpolation functions, and thus the variations of the moduli values are not considered. This highlights The advantage of SEM in analyzing wave dynamics in viscoelastic media as compared to the standard FEM.

Another advantage of SEM follows from the fact that the SEM shape functions are the solutions to the wave equations, so the viscoelastic moduli entering these functions can provide accurate responses instantly. In the FEM, the viscoelastic moduli only appear in the constitutive matrix that requires updating this matrix at each step of the solution procedure and results in vastly increased computational costs [77]. These differences are especially pronounced in dynamic problems. Fig. 4 illustrates the variation of the SEM shape functions with frequency (Fig. 4(b)) in comparison with the FEM shape functions that remain unchanged, enabling thus to accurately capture only static behavior Fig. 4(d). To overcome this issue, the FEM requires a sufficiently large number of elements to resolve the dynamic response governed by the frequency. This puts strict requirements on the mesh density (the mesh should properly resolve the waves at the highest analyzed frequency) resulting in (extremely) fine-meshed models in a high-frequency range. This is not the case for the SEM models.

3. The SEM procedure for a viscoelastic metamaterial plate

In this section, we apply the proposed SEM formulation to model the wave dynamics in a polymer metamaterial plate. The metamaterial unit cell is shown in Fig. 5(a), where four rods of 1 mm thick with rectangular cross-sections are connected to a central cylindrical disk of 28 mm diameter. The height in the vertical direction is 10 mm. The lattice vectors $\boldsymbol{a}_1$ and $\boldsymbol{a}_2$ ($\|\boldsymbol{a}_1\| = \|\boldsymbol{a}_2\| = a = 40$ mm) are aligned with x and y directions, respectively. For the square lattice of the unit cells we use a triangular IBZ for the band structure analysis [78] as shown in Fig. 5(b).

The host material is polycarbonate, which is a durable and tough thermoplastic with a glass transition temperature above 150 °C. Polycarbonate shows viscoelastic properties at room temperature due to secondary transitions in the glassy state [79]. To estimate the effects of the secondary viscous losses, which are often neglected, we model the plate as an elastic and viscoelastic solid. Polycarbonate has a material density of 1185 kg/m^3, elastic modulus 2.17 GPa, and a Poisson's ratio of 0.375. Its viscoelastic behavior can be represented by Prony series (2) with the two sets of values for the relaxation modulus and relaxation time: (0.356 GPa, 0.618 s) and (0.15 GPa, 0.0996 s). Noteworthy, as the Poisson's ratio is also a time (or frequency)-dependent material function in the case of the viscoelastic material, its constant approximation could introduce variations in the dynamic behavior. Although in this study, we have selected a constant Poisson's ratio for polycarbonate [80], it is possible to account for its variability via Eq. (2).

According to the formulation of the SEM procedure (Fig. 1), we need to represent the plate geometry by means of the SEM frame elements. For this, we note that the stiffness of the central disk is considerably higher than that of the surrounding rods meaning that the eigenfrequencies of the disk should also be high. At low frequencies, *i.e.,* around the first band gap, the dynamics of the metamaterial is thus governed by wave scattering in the thin ligaments [76,81], and we can assume that the geometry of the disk is not relevant. The 28 mm diameter disk can then be replaced with a square prism shown in Fig. 5(b), one side of which has a dimension of $b = 20$ mm and the length of the side at the four corners reduces to $b-2d$ with $d = 2.7$ mm; the height of the unit cell is preserved.

Eventual discrepancies due to the modification of the unit-cell geometry can be estimated by comparing band structure diagrams for the original and modified unit cells given in Figs. 5(c) and 5(d), respectively, under the assumption of lossless (elastic) material behavior. The two band structures have a band gap (shaded region) that spans from $f_1 = 5.8$ kHz to $f_2 = 13.75$ kHz with some localized modes in between. The eigenmodes at f_1 are similar for the two geometries and governed by the bending of the ligaments with no contribution from the disk. The localized modes within the first band gap are also governed by

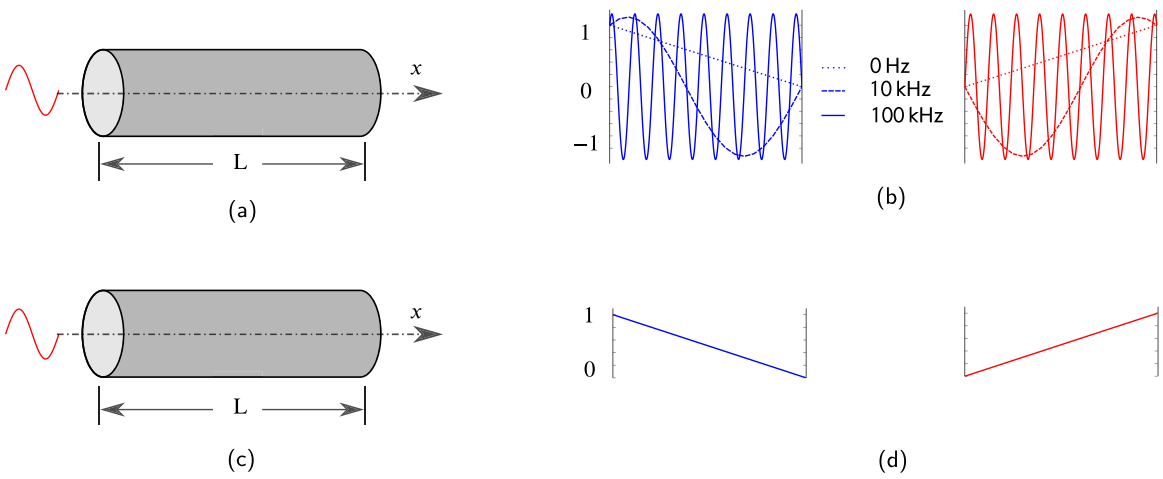

Fig. 4. Comparison of SEM and FEM shape functions at different frequencies: (a), (c) schematics of a traveling wave through a cylindrical rod for both methods; (b) SEM shape functions at the indicated frequencies; (d) FEM linear shape functions.

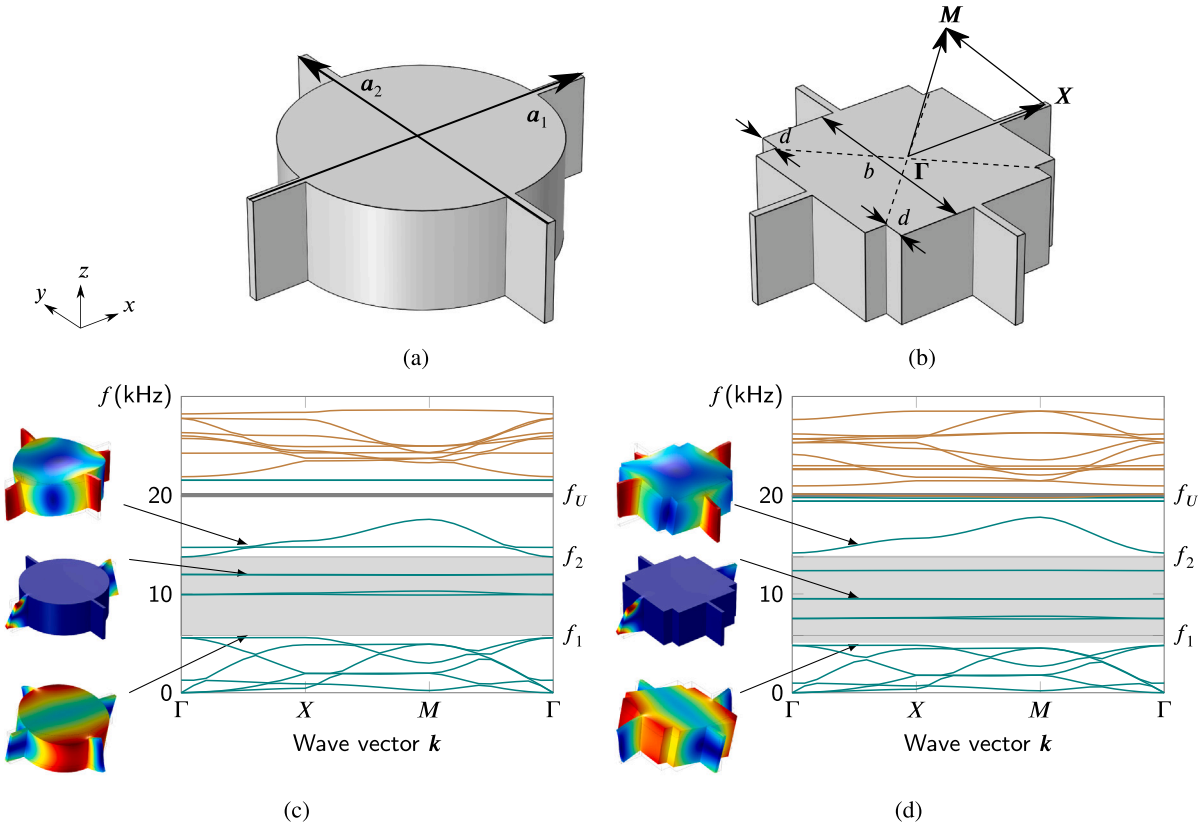

Fig. 5. (a) Unit cell of the metamaterial plate with lattice vectors $\boldsymbol{a}_1$ and $\boldsymbol{a}_2$ aligned to x and y directions. (b) The modified unit cell, where the central disk is replaced with a square prism, and the corresponding IBZ is marked with arrows. The dashed lines separate the prism into four identical parts that can be represented by SEM frame elements. (c–d) Band structures and selected eigenmodes for the two unit cells. As can be seen, the two structures are identical below the first band gap indicated by the shaded region between $f_1 = 5.8\,\text{kHz}$ and $f_2 = 13.75\,\text{kHz}$. The frequency range of interest is marked by gray solid lines and reached $f_U = 20\,\text{kHz}$ in both band structures. The displacement modes correspond to f_1, f_2, and a localized mode within the band gap are similar for the two unit cells. The bands with the similar dynamics for both models are marked in teal, the other bands are depicted in brown.

the bending of the ligaments. These modes, however, have negligible influence on the wave propagation characteristics in the plate and are thus not considered further. Note that the frequencies and curvature of the passbands up to 20 kHz (marked as f_U) are almost identical in the two diagrams with some differences appearing at higher frequencies. The high-frequency variations are due to the interaction of the higher-order eigenmodes of the disk (prism) with those of the ligaments as can already be seen for the mode at f_2. The latter mode is governed by the bending of the disk (prism), but since the mass of the central elements is identical, the variations in the corresponding wavebands are negligible. Therefore, the proposed approximation of the original unit cell geometry is appropriate to analyze the wave dynamics, *i.e.,* up to 20 kHz (which includes the first band gap).

Next, the central square (bulk portion) is converted to four SEM frame elements joined at the center with the separation shown by the

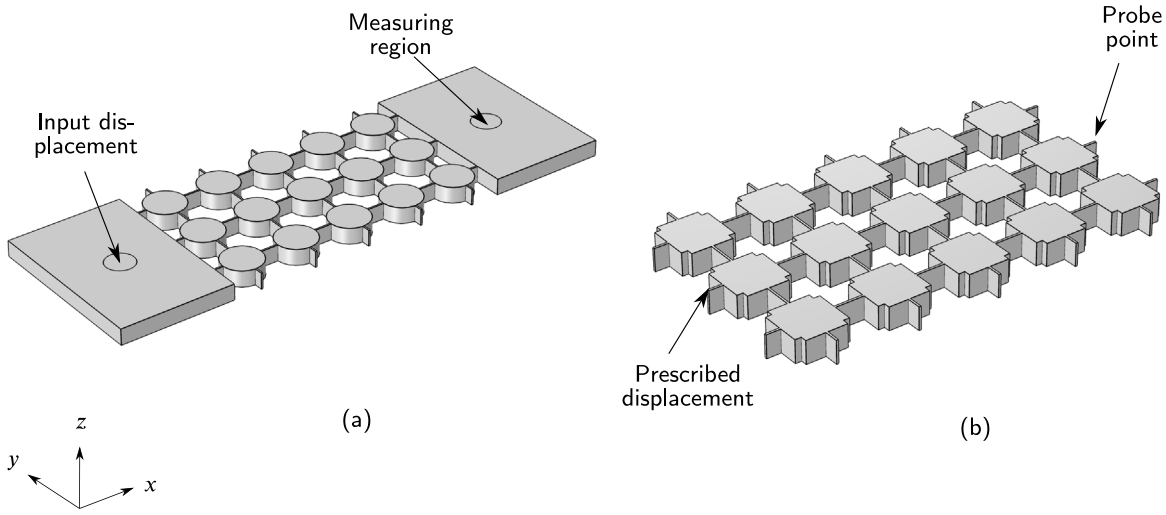

Fig. 6. (a) The model of the metamaterial plate for the transmission analysis with indicated excitation and output regions, (b) The generated SEM model of the plate with equivalent boundary conditions.

dashed lines in Fig. 5(b). This is necessary because the SEM frame element cannot represent a bulk geometry by a two-node one-dimensional element shown in Fig. 2. After the separation, the four frame elements can capture most of the modes of the central bulk region due to a large number of the available DOFs (3 translation and 3 rotation DOFs per each frame element). Further, we represent the four ligaments in the original unit cell with the rod frame elements and finally obtain an equivalent SEM model of the unit cell. The SEM unit cell is tessellated to form an equivalent metamaterial plate (Fig. 6(b)) representing the original plate design (Fig. 6(a)).

The derived SEM model of the metamaterial plate has only 120 frame elements (8 elements per unit cell ×15 unit cells). For comparison, we developed an FEM model that has 168519 tetrahedral elements required to analyze the target frequency range. Hence, the computational advantage of the SEM model is obvious.

As explained, the wave dynamics of the viscoelastic plate is analyzed by replacing the elastic moduli with their complex-valued counterparts expressed by Prony series [82]. Note that despite one typically requires a large number of the elements in the Prony series to properly capture the material viscoelasticity [83], this is not the case for the SEM model. It is because the 3D structural viscoelasticity allowing all types of modes and their interactions is replaced by considering 1D elements that restrict the motion to specific modes corresponding to the allowed DOFs.

3.1. Experimental setup for transmission experiments

The metamaterial plate is fabricated from a transparent polycarbonate sheet of 10 mm thickness. The pattern was introduced via milling (Benchman VMC 4000). The final configuration of the plate specimen has a metamaterial part with 3 × 5 unit cells and two homogeneous parts with dimensions 120 mm × 200 mm.

The experimental setup to measure wave transmission in the plate includes a bi-morphic piezoelectric PZT disk of 10 mm diameter glued to a surface of a homogeneous part of the plate (Fig. 7) that acts as an actuator. The actuator connected to the signal generator and high-voltage amplifier (OPA547-TI) applies vertical excitation in the target frequency range (Fig. 6). Another PZT disk of the same diameter is glued symmetrically at the opposite side of the meta-structure, on the other homogeneous part, and acts as a sensor. This sensor is connected to oscilloscope RTM3000 with a sample rate of 5G samples/s for acquiring the transmitted signal. The sample is placed on a foam bed to isolate it from environmental vibrations without affecting its dynamic response.

4. Results and discussion

4.1. Numerical vs experimental viscoelastic response

Fig. 8 shows the comparison between the calculated (SEM) and measured transmission response with the predicted band gap shaded in gray. The experimental transmission is estimated as the ratio of voltages between the piezo sensor (V_{out}) and the piezo actuator (V_{in}) obtained using the gain function:

$$\text{Gain} = 20 \times \log_{10}\left(\frac{V_{out}}{V_{in}}\right). \tag{13}$$

Comparing the theoretical and experimental data, we see that SEM can adequately predict the transmission around the first band gap that spans from $f_L = 10.25\,\text{kHz}$ to $f_U = 20.5\,\text{kHz}$. This frequency range significantly differs from that for the undamped case shown in Fig. 5(c). Therefore, we can state that the material viscoelasticity shifts the first band gap to higher frequencies (the lower band-gap band is moved from 7 kHz to 10.25 kHz) and increases its width (the upper band-gap bound is shifted from 13.75 kHz to 20.5 kHz). At frequencies above 20 kHz, the variation between the SEM and experimental results increases due to the contribution of the disk's eigenmodes, which are not properly captured by the SEM frame elements. Another limitation of the SEM approximation is the impossibility of predicting experimentally observed transmission peaks and dips because the three-dimensional dynamics of the plate are modeled by one-dimensional elements and due to the complexity of the viscoelastic material behavior, as discussed below. Note that FEM models also suffer from a similar drawback [76]. Additionally, as described in Section 2.2, the variations in the viscoelastic moduli are not accounted for by the interpolation functions in FEM models, which further increases the number of evaluation steps and hence the computational cost compared to the SEM counterpart.

The dynamic behavior of viscoelastic (meta)material can be accurately predicted provided the viscoelastic moduli adequately capture experimental master curves that typically require many elements in the corresponding Prony series (2) depending on the target frequency range and its proximity to the primary and secondary transition zones [76]. In our case, the difference in the storage and loss moduli values between the approximated and experimental master curves are significant (Fig. 9). The theoretical master curves are constructed by using two elements of the series, while the experimental curves are generated via the dynamic temperature-mechanical analysis (DMT) [76]. As a result, the storage modulus curves match only at low frequencies (close to 0.0001 kHz) and strongly deviate from each other at higher frequencies.

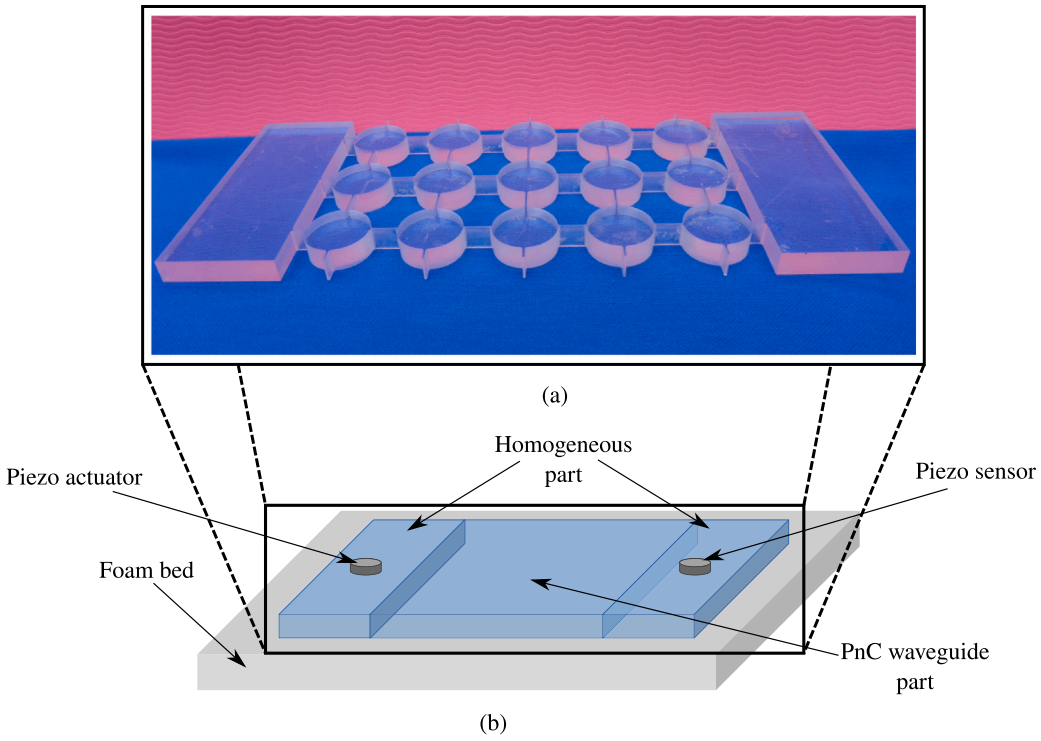

Fig. 7. Schematic of the experimental setup to measure the transmission in the metamaterial plate: (a) the photograph of the plate placed on a foam bed to isolate it from environmental vibrations; (b) schematics of the experimental setup with the piezo-actuator to apply harmonic excitation and the piezo-sensor to detect transmitted waves.

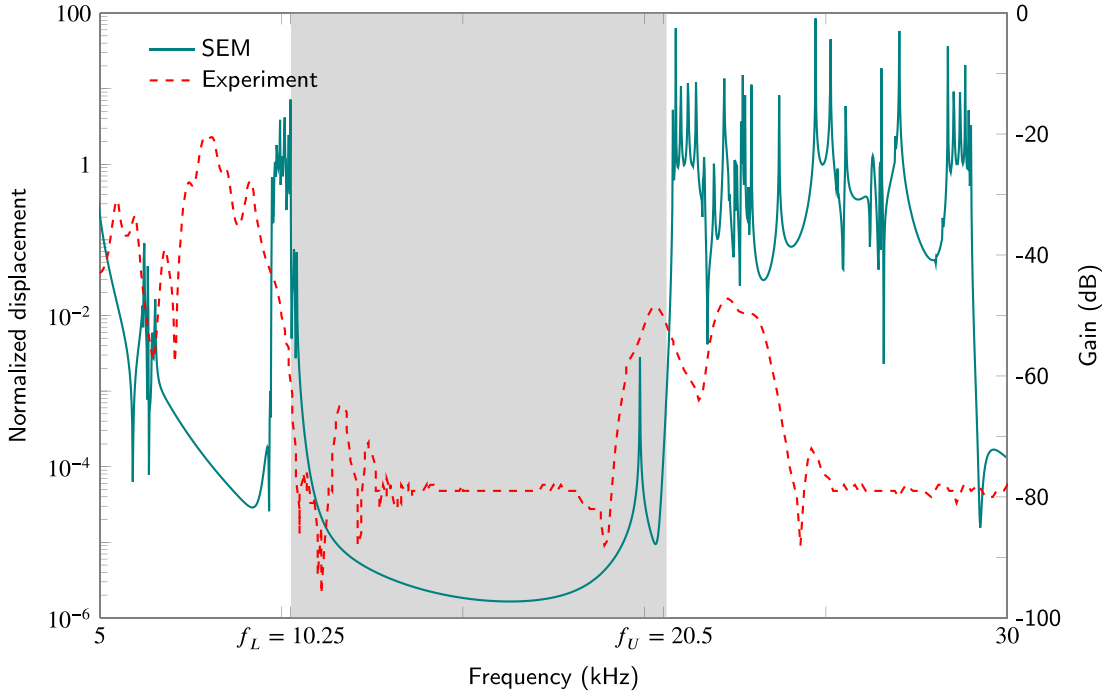

Fig. 8. Theoretical (green) and experimental (dashed red) transmission values for the polycarbonate metamaterial plate. The theoretical data are represented using normalized displacement ((the left y-axis), while the experimental data is plotted by using a gain function (the right y-axis). The shaded region is the predicted band gap bounded by frequencies f_L and f_U.

In the target frequency range (the shaded region: 5 kHz–20 kHz), the theoretical storage modulus is about 18% higher as compared to the experimental value. Besides, the theoretical storage modulus remains constant, while the experimental one increases with frequency in a non-uniform way (see the inset in Fig. 9(a)). The experimental loss modulus shows negligible variation with the frequency with close to zero values at room temperature. In contrast, the theoretical loss modulus has a Gaussian-type shape with a peak around 0.001 kHz. However, the loss modulus values remain very small at the target frequencies implying an insignificant effect on the dynamic response of the plate. Additionally, as described in Section 3, the Poisson's ratio is assumed as a constant value corresponding to the metamaterial plate's equilibrium behavior,

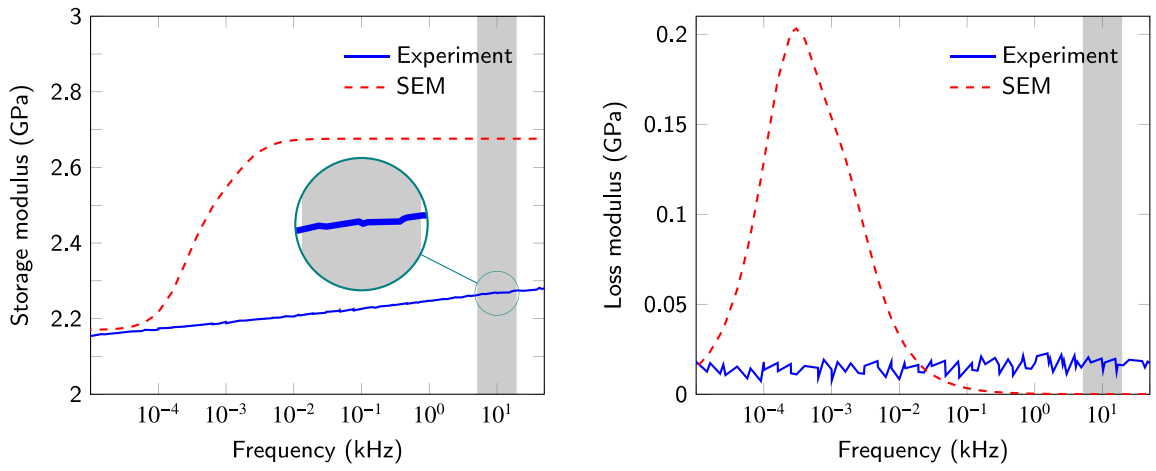

(a) (b)

Fig. 9. SEM and experimental master curve at room temperature (20 °C) with the shaded region indicating the target frequency range: (a) storage modulus and (b) loss modulus. The inset in (a) shows the presence of localized peaks and dips in the experimentally measured storage modulus.

which introduces further error in estimating its transmission peaks response.

The discussed differences between the theoretical and experimental master curves and the use of 1D frame elements to approximate the 3D geometry hinder the SEM model from accurately predicting the wave transmission in the considered plate. However, increasing the number of the components in the Prony series in order to improve the match with the experimental master curves might not necessarily improve the performance of the SEM model due to its intrinsic one-dimensional nature. Nevertheless, despite this restriction, the SEM model provides surprisingly accurate predictions around the first band gap that can be challenging even for the computationally expensive FEM models [76]. Therefore, we conclude that this model can be successfully used as a first-hand approximation to design and optimize viscoelastic metamaterial structures at frequencies close to the first band gap.

5. Summary and conclusions

In this work, we proposed an analytical procedure based on the spectral element method (SEM) to characterize the wave dynamics of bulk (3D) and plate-like (2D) viscoelastic metamaterials. We discussed how to approximate a metamaterial's 3D geometry by means of 1D SEM frame elements. The accuracy of the approximation was estimated by studying the band structures of both the original and simplified unit cells, and such accuracy was shown to be adequate at frequencies around the first band gap. The wave transmission predicted by the SEM model was also validated experimentally for a polycarbonate metamaterial plate. The obtained results allow us to draw the following conclusions:

- The dynamic analysis of dissipative metamaterials is intricate due to frequency-dependent viscoelastic effects that increase the computational costs when employing standard computational tools such as finite element analysis. Analytical models, such as the proposed extension of SEM, can partially solve this issue depending on the target frequency range. Since SEM incorporates frequency dependence in its shape functions, fine meshes are not required. Additionally, linear viscoelastic behavior can easily be introduced into the SEM elements by modifying the shape functions, which further simplifies the analysis and reduces the computational costs;
- The obtained accurate match between the SEM and experimental results for the wave transmission in the plate suggests that SEM models can provide reliable approximations by significantly reducing the simulation time for plate-like viscoelastic metamaterials at frequencies around the first band gap at the cost of introducing a simplified geometry for a plate;
- The limitation of SEM, *i.e.*, its inability to deal with complex geometries, can be overcome in practice by developing approximate models in 2D and 3D by assembling 1D (beam/frame) elements, which would be accurate for specific frequency ranges. Moreover, depending on complexities in the geometry, the number and arrangement of 1D elements can be defined. This approach provides the designer with a back-of-envelope method/tool for quick analysis of these structures, which is otherwise very tedious. SEM models are very effective in determining accurately the first band gap. This allows us to easily test many materials (changing the properties of the base material) and any number of the metamaterial's unit cells. This can therefore make SEM the methodology of choice to quickly prototype new metamaterials irrespective of their field of application.

As a future direction, complex structural elements such as plates/shells can be incorporated into the SEM-based viscoelastic model to represent the behavior of intricate geometries accurately. This modification will also aid in incorporating more Maxwell elements into the Prony series as plates/shells possess complex displacement modes allowing them to accurately mimic the response from DMTA. Additionally, an SEM–FEM *hybrid* method [59] that leverages both advantages can be used to model viscoelastic metamaterials with complex geometries.

CRediT authorship contribution statement

Sabiju Valiya Valappil: Conceptualization, Methodology, Software, Writing – original draft. **Anastasiia O. Krushynska:** Conceptualization, Supervision, Experimental validation, Writing – review & editing. **Alejandro M. Aragón:** Conceptualization, Investigation, Supervision, Writing – review & editing.

Declaration of competing interest

The authors declare that they have no known competing financial interests or personal relationships that could have appeared to influence the work reported in this paper.

Data availability

Data will be made available on request.

Acknowledgments

The authors greatly appreciate the financial support from the top-consortium voor kennis en innovatie (TKI) grant and our funding partner KROHNE, Netherlands. Additionally, the authors are deeply thankful to Dr. M. Acuautla and M. Stokroos from the Engineering and Technology Institute Groningen for their technical support and for providing access to the machines for performing the experiments. The authors also acknowledge the group of Prof. N. M. Pugno from the University of Trento in Italy for manufacturing the sample.

References

[1] Stephen H. Crandall, The role of damping in vibration theory, J. Sound Vib. 11 (1) (1970) 3–IN1.
[2] D.H. Wang, W.H. Liao, Semi-active suspension systems for railway vehicles using magnetorheological dampers. Part I: system integration and modelling, Veh. Syst. Dyn. 47 (11) (2009) 1305–1325.
[3] Feilong Xu, Liang Sun, Liang Zhen, X. He, Z. Yang, Decorated membrane resonators as underground seismic wave barriers against high magnitude earthquakes, J. Appl. Phys. 128 (8) (2020) 084902.
[4] S.S. Iyer, R. Vedad-Ghavami, H. Lee, M. Liger, H.P. Kavehpour, R.N. Candler, Nonlinear damping for vibration isolation of microsystems using shear thickening fluid, Appl. Phys. Lett. 102 (25) (2013) 251902.
[5] Ioannis Politopoulos, A review of adverse effects of damping in seismic isolation, Earthq. Eng. Struct. Dyn. 37 (3) (2008) 447–465.
[6] Hadi Najar, Mei-Lin Chan, Hsueh-An Yang, Liwei Lin, David G. Cahill, David A. Horsley, High quality factor nanocrystalline diamond micromechanical resonators limited by thermoelastic damping, Appl. Phys. Lett. 104 (15) (2014) 151903.
[7] Marko Mihalec, Jaka Javh, Filippo Cianetti, Michele Moretti, Gianluca Rossi, Janko Slavič, Miha Boltežar, Damping heat coefficient–theoretical and experimental research on a vibrating beam, J. Sound Vib. 400 (2017) 13–21.
[8] Thomas H. Metcalf, Bradford B. Pate, Douglas M. Photiadis, Brian H. Houston, Thermoelastic damping in micromechanical resonators, Appl. Phys. Lett. 95 (6) (2009) 061903.
[9] F.R. Schwarzl, Numerical calculation of storage and loss modulus from stress relaxation data for linear viscoelastic materials, Rheol. Acta 10 (2) (1971) 165–173.
[10] Roderic Lakes, Roderic S. Lakes, Viscoelastic Materials, Cambridge University Press, 2009.
[11] M.S. Kushwaha, P. Halevi, L. Dobrzynski, B. Djafari-Rouhani, Acoustic band structure of periodic elastic composites, Phys. Rev. Lett. 71 (1993) 2022–2025.
[12] W.L. Bragg, The diffraction of short electromagnetic waves by a crystal, Scientia 23 (45) (1929) 153.
[13] Steven A. Cummer, Johan Christensen, Andrea Alù, Controlling sound with acoustic metamaterials, Nat. Rev. Mater. 1 (3) (2016) 16001.
[14] Matthew Reynolds, Stephen Daley, An active viscoelastic metamaterial for isolation applications, Smart Mater. Struct. 23 (4) (2014) 045030.
[15] A.A. Maznev, A.G. Every, O.B. Wright, Reciprocity in reflection and transmission: What is a 'phonon diode'? Wave Motion 50 (4) (2013) 776–784.
[16] Osama R. Bilal, André Foehr, Chiara Daraio, Bistable metamaterial for switching and cascading elastic vibrations, Proc. Natl. Acad. Sci. 114 (18) (2017) 4603–4606.
[17] Kyung Ho Sun, Jae Eun Kim, Jedo Kim, Kyungjun Song, Sound energy harvesting using a doubly coiled-up acoustic metamaterial cavity, Smart Mater. Struct. 26 (7) (2017) 075011.
[18] Shu Zhang, Leilei Yin, Nicholas Fang, Focusing ultrasound with an acoustic metamaterial network, Phys. Rev. Lett. 102 (19) (2009) 194301.
[19] Choon Mahn Park, Jong Jin Park, Seung Hwan Lee, Yong Mun Seo, Chul Koo Kim, Sam H. Lee, Amplification of acoustic evanescent waves using metamaterial slabs, Phys. Rev. Lett. 107 (2011) 194301.
[20] Chengrong Ma, Shuxiang Gao, Ying Cheng, Xiaojun Liu, Acoustic metamaterial antennas for combined highly directive-sensitive detection, Appl. Phys. Lett. 115 (5) (2019) 053501.
[21] J. Xu, J. Tang, Tunable prism based on piezoelectric metamaterial for acoustic beam steering, Appl. Phys. Lett. 110 (18) (2017) 181902.
[22] Hyuk Lee, Jun Kyu Lee, Hong Min Seung, Yoon Young Kim, Mass-stiffness substructuring of an elastic metasurface for full transmission beam steering, J. Mech. Phys. Solids 112 (2018) 577–593.
[23] Shu Zhang, Chunguang Xia, Nicholas Fang, Broadband acoustic cloak for ultrasound waves, Phys. Rev. Lett. 106 (2) (2011) 024301.
[24] Mohamed Farhat, Sebastien Guenneau, Stefan Enoch, Ultrabroadband elastic cloaking in thin plates, Phys. Rev. Lett. 103 (2) (2009) 024301.
[25] Nicolas Stenger, Manfred Wilhelm, Martin Wegener, Experiments on elastic cloaking in thin plates, Phys. Rev. Lett. 108 (1) (2012) 014301.
[26] H.K. Zhang, Yi Chen, X.N. Liu, G.K. Hu, An asymmetric elastic metamaterial model for elastic wave cloaking, J. Mech. Phys. Solids 135 (2020) 103796.
[27] Fabrice Lemoult, Mathias Fink, Geoffroy Lerosey, Acoustic resonators for far-field control of sound on a subwavelength scale, Phys. Rev. Lett. 107 (6) (2011) 064301.
[28] Y.P. Zhao, P.J. Wei, The band gap of 1D viscoelastic phononic crystal, Comput. Mater. Sci. 46 (3) (2009) 603–606, Proceedings of the 18th International Workshop on Computational Mechanics of Materials.
[29] Joo Hwan Oh, Yoon Jae Kim, Yoon Young Kim, Wave attenuation and dissipation mechanisms in viscoelastic phononic crystals, J. Appl. Phys. 113 (10) (2013) 106101.
[30] Gang Wang, Jihong Wen, Yaozong Liu, Xisen Wen, Lumped-mass method for the study of band structure in two-dimensional phononic crystals, Phys. Rev. B 69 (2004) 184302.
[31] Jianbao Li, Yue-Sheng Wang, Chuanzeng Zhang, Finite element method for analysis of band structures of three dimensonal phononic crystals, in: 2008 IEEE Ultrasonics Symposium, 2008, pp. 1468–1471.
[32] Yong Xiao, Jihong Wen, Gang Wang, Xisen Wen, Theoretical and experimental study of locally resonant and bragg band gaps in flexural beams carrying periodic arrays of beam-like resonators, J. Vib. Acoust. 135 (4) (2013) 041006.
[33] Mahmoud I. Hussein, Michael J. Frazier, Band structure of phononic crystals with general damping, J. Appl. Phys. 108 (9) (2010) 093506.
[34] Mahmoud I. Hussein, Michael J. Frazier, Metadamping: An emergent phenomenon in dissipative metamaterials, J. Sound Vib. 332 (20) (2013) 4767–4774.
[35] Michael J. Frazier, Mahmoud I. Hussein, Viscous-to-viscoelastic transition in phononic crystal and metamaterial band structures, J. Acoust. Soc. Am. 138 (5) (2015) 3169–3180.
[36] Michael J. Frazier, Mahmoud I. Hussein, Generalized Bloch's theorem for viscous metamaterials: Dispersion and effective properties based on frequencies and wavenumbers that are simultaneously complex, C. R. Phys. 17 (5) (2016) 565–577.
[37] Raj K. Narisetti, Massimo Ruzzene, Michael J. Leamy, Study of wave propagation in strongly nonlinear periodic lattices using a harmonic balance approach, Wave Motion 49 (2) (2012) 394–410.
[38] G.L. Huang, C.T. Sun, Band gaps in a multiresonator acoustic metamaterial, J. Vib. Acoust. 132 (3) (2010) 031003.
[39] P. Frank Pai, Metamaterial-based broadband elastic wave absorber, J. Intell. Mater. Syst. Struct. 21 (5) (2010) 517–528.
[40] Y.Y. Chen, G.L. Huang, C.T. Sun, Band gap control in an active elastic metamaterial with negative capacitance piezoelectric shunting, J. Vib. Acoust. 136 (6) (2014).
[41] Kwek Tze Tan, H.H. Huang, C.T. Sun, Blast-wave impact mitigation using negative effective mass density concept of elastic metamaterials, Int. J. Impact Eng. 64 (2014) 20–29.
[42] Dongwoo Lee, Minkyung Kim, Junsuk Rho, A finite element method towards acoustic phononic crystals by weak formulation, J. Phys.: Condens. Matter 31 (37) (2019) 375901.
[43] Rixin Cui, Jinsong Zhou, Dao Gong, Band gap and vibration reduction properties of damped rail with two-dimensional honeycomb phononic crystals, Shock Vib. 2021 (2021) 8814962.
[44] K. Billon, M. Ouisse, E. Sadoulet-Reboul, M. Collet, P. Butaud, G. Chevallier, A. Khelif, Design and experimental validation of a temperature-driven adaptive phononic crystal slab, Smart Mater. Struct. 28 (3) (2019) 035007.
[45] Yuanchao Zhang, Wei Xu, Chiming Wang, Zhengmin Li, Jianwei Cheng, Shengwu Zhang, Modeling and experimental analysis of particle damping phononic crystal plate, AIP Adv. 11 (10) (2021) 105202.
[46] Romik Khajehtourian, Dennis M. Kochmann, A continuum description of substrate-free dissipative reconfigurable metamaterials, J. Mech. Phys. Solids (2020) 104217.
[47] A.O. Krushynska, V.G. Kouznetsova, M.G.D. Geers, Visco-elastic effects on wave dispersion in three-phase acoustic metamaterials, J. Mech. Phys. Solids 96 (2016) 29–47.
[48] M.A. Lewińska, V.G. Kouznetsova, J.A.W. van Dommelen, A.O. Krushynska, M.G.D. Geers, The attenuation performance of locally resonant acoustic metamaterials based on generalised viscoelastic modelling, Int. J. Solids Struct. 126 (2017) 163–174.
[49] Yan-Feng Wang, Yue-Sheng Wang, Vincent Laude, Wave propagation in two-dimensional viscoelastic metamaterials, Phys. Rev. B 92 (10) (2015) 104110.
[50] P. Langer, M. Maeder, C. Guist, M. Krause, S. Marburg, More than six elements per wavelength: The practical use of structural finite element models and their accuracy in comparison with experimental results, J. Comput. Acoust. 25 (04) (2017) 1750025.
[51] Linlin Shi, Yuanguo Zhou, Jia-Min Wang, Mingwei Zhuang, Na Liu, Qing Huo Liu, Spectral element method for elastic and acoustic waves in frequency domain, J. Comput. Phys. 327 (2016) 19–38.
[52] Linlin Shi, Na Liu, Jianyang Zhou, Yuanguo Zhou, Jiamin Wang, Qing Huo Liu, Spectral element method for band-structure calculations of 3D phononic crystals, J. Phys. D: Appl. Phys. 49 (45) (2016) 455102.

[53] Anthony T. Patera, A spectral element method for fluid dynamics: laminar flow in a channel expansion, J. Comput. Phys. 54 (3) (1984) 468–488.
[54] Dimitri Komatitsch, Jean-Pierre Vilotte, The spectral element method: an efficient tool to simulate the seismic response of 2D and 3D geological structures, Bull. Seismol. Soc. Am. 88 (2) (1998) 368–392.
[55] James F. Doyle, Wave propagation in structures, in: Wave Propagation in Structures, Springer, 1989, pp. 126–156.
[56] Henri J. Nussbaumer, The fast Fourier transform, in: Fast Fourier Transform and Convolution Algorithms, Springer Berlin Heidelberg, Berlin, Heidelberg, 1981, pp. 80–111.
[57] Usik Lee, Hyuckjin Oh, The spectral element model for pipelines conveying internal steady flow, Eng. Struct. 25 (8) (2003) 1045–1055.
[58] Usik Lee, Hyungmi Oh, Dynamics of an axially moving viscoelastic beam subject to axial tension, Int. J. Solids Struct. 42 (8) (2005) 2381–2398.
[59] Usik Lee, Spectral Element Method in Structural Dynamics, John Wiley & Sons, 2009.
[60] Yong Xiao, Jihong Wen, Xisen Wen, Longitudinal wave band gaps in metamaterial-based elastic rods containing multi-degree-of-freedom resonators, New J. Phys. 14 (3) (2012) 033042.
[61] Yong Xiao, Jihong Wen, Gang Wang, Xisen Wen, Theoretical and experimental study of locally resonant and bragg band gaps in flexural beams carrying periodic arrays of beam-like resonators, J. Vib. Acoust. 135 (4) (2013).
[62] Filippo Casadei, Katia Bertoldi, Wave propagation in beams with periodic arrays of airfoil-shaped resonating units, J. Sound Vib. 333 (24) (2014) 6532–6547.
[63] E.D. Nobrega, F. Gautier, A. Pelat, J.M.C. Dos Santos, Vibration band gaps for elastic metamaterial rods using wave finite element method, Mech. Syst. Signal Process. 79 (2016) 192–202.
[64] Muhammad, Weijian Zhou, C.W. Lim, Topological edge modeling and localization of protected interface modes in 1D phononic crystals for longitudinal and bending elastic waves, Int. J. Mech. Sci. 159 (2019) 359–372.
[65] C.W. Lim, et al., Analytical modeling and computational analysis on topological properties of 1-D phononic crystals in elastic media, J. Mech. Mater. Struct. 15 (1) (2020) 15–35.
[66] Richard Christensen, Theory of Viscoelasticity: An Introduction, Elsevier, 2012.
[67] Felix Bloch, Über die quantenmechanik der elektronen in kristallgittern, Z. Phys. 52 (7–8) (1929) 555–600.
[68] Thomas J.R. Hughes, The Finite Element Method: Linear Static and Dynamic Finite Element Analysis, Courier Corporation, 2012.
[69] Jean H. Prévost, Serguei Bagrianski, An Introduction To Matrix Structural Analysis and Finite Element Methods, World Scientific, 2017.
[70] Yudong Zhang, Leiying He, Chuanyu Wu, The effect of preload force on damping in tendon-driven manipulator, Ind. Robot: Int. J. Robot. Res. Appl. 48 (3) (2021) 454–462.
[71] Paul Macioce, Viscoelastic damping 101, Sound Vibrat. Mag. 4 (2003) 4–5.
[72] R. Lewandowski, B. Chorążyczewski, Identification of the parameters of the Kelvin–Voigt and the Maxwell fractional models, used to modeling of viscoelastic dampers, Comput. Struct. 88 (1) (2010) 1–17.
[73] Émilie Blanc, Dimitri Komatitsch, Emmanuel Chaljub, Bruno Lombard, Zhinan Xie, Highly accurate stability-preserving optimization of the Zener viscoelastic model, with application to wave propagation in the presence of strong attenuation, Geophys. J. Int. 205 (1) (2016) 427–439.
[74] Franck Renaud, Jean-Luc Dion, Gaël Chevallier, Imad Tawfiq, Rémi Lemaire, A new identification method of viscoelastic behavior: Application to the generalized Maxwell model, Mech. Syst. Signal Process. 25 (3) (2011) 991–1010.
[75] G. Casula, J.M. Carcione, et al., Generalized mechanical model analogies of linear viscoelastic behaviour, Bollettino di geofisica teorica ed applicata 34 (136) (1992) 235–256.
[76] Anastasiia O. Krushynska, Nitesh Anerao, Miguel A. Badillo-Ávila, Martin Stokroos, Mónica Acuautla, Arbitrary-curved waveguiding and broadband attenuation in additively manufactured lattice phononic media, Mater. Des. 205 (2021) 109714.
[77] Bruno Jurkiewiez, Jean-François Destrebecq, Alain Vergne, Incremental analysis of time-dependent effects in composite structures, Comput. Struct. 73 (1) (1999) 425–435.
[78] Fengfeng Shu, Yongshun Liu, Junfeng Wu, Yihui Wu, Band gap in tubular pillar phononic crystal plate, Ultrasonics 71 (2016) 172–176.
[79] Anastasiia O. Krushynska, Antonio S. Gliozzi, Alberto Fina, Dmitry Krushinsky, Daniele Battegazzore, Miguel A. Badillo-Ávila, Mónica Acuautla, Stefano Stassi, Camilla Noè, Nicola M. Pugno, Federico Bosia, Dissipative dynamics of polymer phononic materials, Adv. Funct. Mater. 31 (30) (2021).
[80] A.H. Tsou, J. Greener, G.D. Smith, Stress relaxation of polymer films in bending, Polymer 36 (5) (1995) 949–954.
[81] A.O. Krushynska, M. Miniaci, F. Bosia, N.M. Pugno, Coupling local resonance with bragg band gaps in single-phase mechanical metamaterials, Extreme Mech. Lett. 12 (2017) 30–36, Frontiers in Mechanical Metamaterials.
[82] D. Jalocha, A. Constantinescu, R. Neviere, Revisiting the identification of generalized maxwell models from experimental results, Int. J. Solids Struct. 67–68 (2015) 169–181.
[83] J.E. Soussou, F. Moavenzadeh, M.H. Gradowczyk, Application of prony series to linear viscoelasticity, Trans. Soc. Rheol. 14 (4) (1970) 573–584.